WPJET2-CPR(17) 18137

K Heinola et al.

Experience on divertor fuel retention after two JET ITER-Like Wall campaigns

Preprint of Paper to be submitted for publication in Proceeding of 16th International Conference on Plasma-Facing Materials and Components for Fusion Applications

This work has been carried out within the framework of the EUROfusion Consortium and has received funding from the Euratom research and training programme 2014-2018 under grant agreement No 633053. The views and opinions expressed herein do not necessarily reflect those of the European Commission.

Experience on divertor fuel retention after two ITER-Like Wall campaigns

K. Heinola[1*], A. Widdowson[2], J. Likonen[3], T. Ahlgren[1], E. Alves[4], C. F. Ayres[2], A. Baron-Wiechec[2], N. Barradas[5], S. Brezinsek[6], N. Catarino[4], P. Coad[2], I. Jepu[7], S. Krat[8,9], A. Lahtinen[1], G. F. Matthews[2], M. Mayer[8] and JET Contributors[†]

EUROfusion Consortium, JET, Culham Science Centre, Abingdon, OX14 3DB, UK
[1]*Department of Physics, University of Helsinki, P.O. Box 64, 00560 Helsinki, Finland*
[2]*CCFE, Culham Science Centre, Abingdon, OX14 3DB, UK*
[3]*VTT, P.O. Box 1000, 02044 VTT, Espoo, Finland*
[4]*Instituto Superior Tecnico, Instituto de Plasmas e Fusao Nuclear, Universidade de Lisboa, 1049-001, Lisboa, Portugal*
[5]*Centro de Ciencias e Tecnologias, Nucleares Instituto Superior Tecnico, Universidade de Lisboa, 2695-066 Bobadela, Portugal*
[6]*Forschungszentrum Julich GmbH, D-52425, Julich, Germany*
[7]*National Institute for Laser, Plasma and Radiation Physics, Bucharest-Magurele 077125, Romania*
[8]*Max-Planck Institut fur Plasmaphysik, D-85748, Garching, Germany and*
[9]*National Research Nuclear University MEPhl, 115409 Moscow, Russia*

The JET ITER-Like-Wall experiment with its all-metal plasma-facing components provides a unique environment for plasma and plasma-wall interaction studies. These studies are of great importance in understanding the underlying phenomena taking place during the operation of a future fusion reactor. Present work summarizes and reports the plasma fuel retention in the divertor resulting from the two first experimental campaigns with the ITER-Like Wall. The deposition pattern in the divertor after the second campaign shows same trend as was observed after the first campaign: highest deposition of $10 - 15$ μm was found on top part of the inner divertor. Due to the change in plasma magnetic configurations from the first to the second campaign, and the resulted strike point locations, an increase of deposition was observed on the base of the divertor. The deuterium retention was found to be affected by the hydrogen plasma experiments done at the end of second experimental campaign.

PACS numbers: 28.52.Fa 52.55.Fa 52.55.Pi 52.70.Nc 52.77.Dq

I. INTRODUCTION

The JET tokamak with its ITER-Like Wall (ILW) project [1] provides a unique opportunity to study the plasma-material interactions (PMI) taking place in operating the next-step fusion device ITER. In ILW, the main chamber limiters comprise of bulk beryllium (Be), and the divertor consists of armour tiles of either bulk tungsten (W), or W-coated carbon-fibre composite (CFC) tiles. Removal and replacement of these plasma-facing components (PFC) during shutdown phases of JET allow post-campaign, or *post-mortem*, analyses to scrutinize the campaign integrated net effects of the PMIs. This work summarizes the present results on fuel retention and deposit formation after two ILW campaigns.

Gas balance measurements performed during the first operational phase of JET-ILW in 2011-2012 (ILW-1) have shown a factor 10-20 reduction in the long-term fuel retention measurements as compared to the operational period 2007-2009 with an all-Carbon wall (JET-C) [2]. The ILW-1 post-mortem analyses of the PFCs retrieved from the JET vessel during the shutdown 2013 mapped the global distribution of the deposits and fuel retention inside the machine ([3–8] and references therein). The global fuel retention rate was found to have decreased in ILW-1 by a factor > 18 as compared to JET-C [5]. Also, the results showed the chemistry affecting the erosion and deposit migration when changing from JET-C to JET-ILW: the deposit formation in ILW does not appear to proceed via long range migration of the eroded particles due to lack of enhanced re-erosion. The highest amounts of metallic deposits were found on top of the inner divertor, whereas in JET-C the thickest C deposits were formed in the base of the divertor due to enhanced re-erosion processes by chemical sputtering [3].

The second ILW campaign in 2013-2014 (ILW-2) had similar characteristics to ILW-1, but focused on high power, high density plasma scenarios. A general review on the two ILW campaigns, and on the corresponding shutdown activities are given in Refs. [9] and [10], respectively. The ILW-2 fuel retention post-mortem analyses took place after receiving samples during the JET shutdown 2015, and the first results have been published in Refs. [11–13]. In the present work, the main findings from the ILW-1 and ILW-2 post-mortem results on fuel retention and deposition formation in the divertor

*Corresponding author *Email*: kalle.heinola@helsinki.fi
[†]See the author list of "Overview of the JET results in support to ITER" by X. Litaudon et al. to be published in Nuclear Fusion Special issue: overview and summary reports from the 26th Fusion Energy Conference (Kyoto, Japan 17 - 22 October 2016)

TABLE I: Main characteristics of the plasmas during the ILW-1 and ILW-2 campaings.

	ILW-1 (2011-2012)	ILW-2 (2013-2014)
limiter phase	6 hrs	5.2 hrs
divertor phase	13 hrs	14.2 hrs
hydrogen (H) campaign	none	0.6 hrs
puffed H (atoms)†	none	$\sim 5.9 \times 10^{24}$
puffed D (atoms)*	$\sim 2.8 \times 10^{26}$	$\sim 6.3 \times 10^{26}$
inner strike point‡	Tile 3	Tile 4
outer strike point‡	Tile 5	Tile 6
total input energy	150.6 GJ	200.5 GJ

† puffed fuel during H campaign only.
* includes restart pulses, gas and pellet injections, neutral beam heating, and disruption protection system puffs.
‡ predominant strike point location. Detailed strike point distribution shown in Fig. 2.

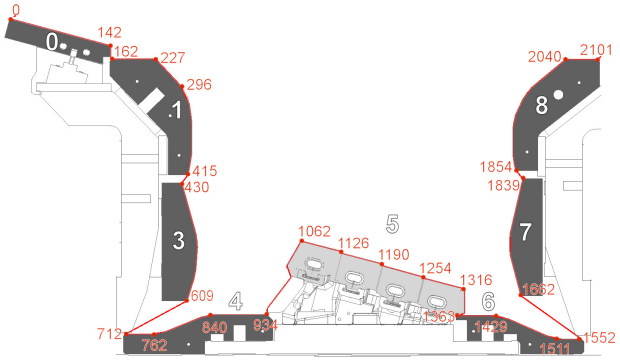

FIG. 1: (Color online) Poloidal cross-section of the ILW divertor. The divertor tiles are numbered (white), and their poloidal locations and geometries are described with divertor S coordinate system (red; in mm's). The W-coated CFC tiles (0, 1, 3, 4, 6, 7, and 8) are highlighted in dark grey, and the bulk W tile (5) in light grey.

are reviewed, and the effect of the plasma operations are discussed.

II. EXPERIMENTAL

A. JET ITER-Like Wall campaigns

The main plasma operation parameters for ILW-1 and ILW-2 are presented in Table I. The total plasma time was approximately identical for both campaigns, but the limiter configuration time was slightly lower in ILW-2 ($\sim$ 5 hrs) than in ILW-1 ($\sim$ 6 hrs), and the divertor configuration time was higher in ILW-2 ($\sim$ 14 hrs) than in ILW-1 ($\sim$ 13 hrs). Both ILW campaigns operated with deuterium (D) plasmas. However, the ILW-2 was finished with a dedicated two-week campaign with hydrogen (H) plasmas (0.6 hrs).

Fig. 1 shows the poloidal cross-section of the ILW divertor, and highlights all the plasma-facing divertor tiles. The plasma strike point distributions on the divertor tiles during ILW-1 and ILW-2 are shown in Fig. 2. The inner divertor strike point (ISP) was mainly on Tile 3 in ILW-1, and on Tile 4 in ILW-2. The outer divertor strike point (OSP) in ILW-1 was mainly in the center tile of divertor on Tile 5, and in ILW-2 it was targeted predominantly on Tile 6.

The amount of puffed D was increased with more than a factor of two in ILW-2. In ILW-1 there were fewer high current, high power pulses with currents up to 3.5 MA, magnetic fields up to 3.2 T, and Neutral Beam Injection (NBI) power up to 26 MW in conjuction with Ion Cyclotron Heating Resonance Heating (ICRH) up to 3.5 MW [14]. The averaged input power was 2.35 MW and the total input energy 150 GJ. In ILW-2 higher number of high current, high power pulses were used with plasma currents up to 4 MA, magnetic field up to 3.7 T, NBI and ICRH up to 27 and 7 MW, respectively, and Lower Hybrid Current Drive Drive heating up to 3 MW [15]. The averaged input power and the total input energy was 2.82 MW and 200 GJ, respectively, resulting to a corresponding increase of 20% and 33% when compared to ILW-1.

B. Post-mortem analyses

1. *Experimental methods*

The ILW divertor comprises of W-coated CFC tiles, and of a bulk W tile (Fig. 1). A special selection of W-coated CFC tiles used in this work have a Mo marker interlayer coating for accurate erosion/deposition studies: a layered coating with a W/Mo/W/Mo/CFC structure, and thicknesses (in μm) of 4/4/12/3/bulk. In addition to the standard bulk W Tile 5's used for analyses, special Mo marker coated bulk W tiles were prepared for the Tile 5 erosion/deposition studies [13].

The post-mortem methodologies applied for both ILW-1 and ILW-2 tile analyses are Ion Beam Analysis (IBA), Thermal Desorption Spectrometry (TDS), and Secondary Ion Mass Spectrometry (SIMS). In IBA, the Nuclear Reaction Analysis (NRA) was used for determining the D concentrations with the D(^{3}He,p)^{4}He nuclear reaction. With NRA also the Be, C impurity concentrations were evaluated with the ^{9}Be(^{3}He,p)^{11}B and ^{12}C(^{3}He,p)^{14}N reactions, respectively. Oxygen (O) was determined by using non-Rutherford scattering cross-sections. The energies used for the ^{3}He ion beam was either 4.5 MeV, or 2.3 MeV. The use of higher ^{3}He energy 4.5 MeV enables D and Be concentration analysis to larger depths, and improves the C and O detection efficiency as the reaction cross-sections increase with projectile ion energy. The 4.5 MeV NRA results were ana-

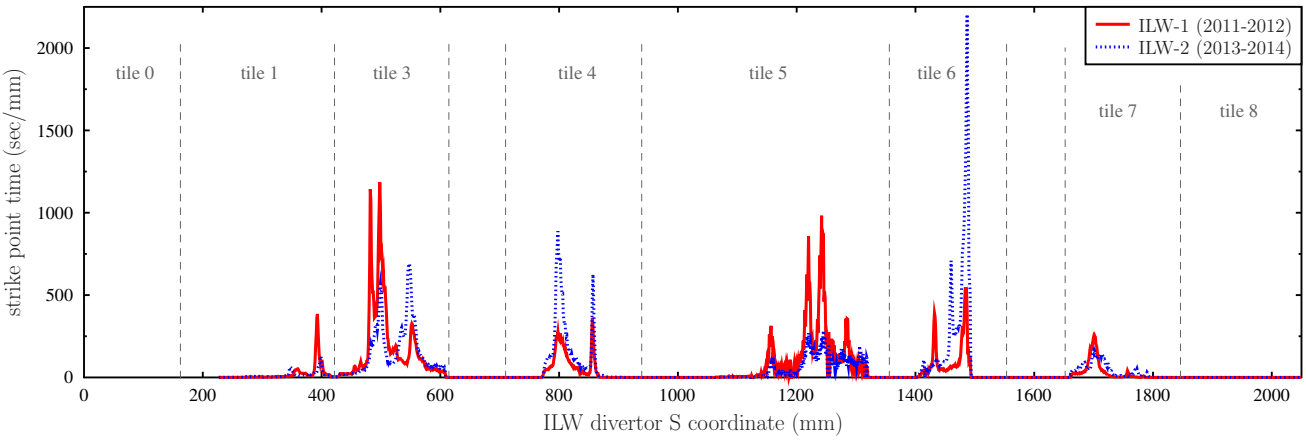

FIG. 2: The plasma strike point residence times in the ILW divertor during the ILW-1 and ILW-2 campaigns as a function of the divertor S coordinate. Corresponding tile locations highlighted.

lyzed the SIMNRA package [16], and the analysis setup is described in Refs. [7, 17]. In conjuction with the 2.3 MeV ^{3}He ion beam for NRA, the Elastic Backscattering (EBS) and Particle Induced X-ray Emission (PIXE) were used for detecting Be and heavier elements. The 2.3 MeV NRA, EBS, and PIXE results were fitted parallelly with WiNDF data furnace software package [18], and the experimental setups are described in detail in Refs. [3, 4, 12].

SIMS analysis was performed for studying the D, Be, C and heavier metallic impurity depth profile concentrations in the ILW divertor samples. The details for the SIMS setup are presented in Refs. [11, 19]. Calibration was done for D by using D-implanted reference samples, which were prepared by implanting 60 keV/D_2 into polycrystalline W, Mo and Be (see details in [20]). The retained D in the implantation-induced defects in the calibration samples was determined with Elastic Recoil Detection Analysis allowing an absolute calibration value for SIMS.

The TDS analyses were done in an ultra-high vacuum system with a background pressure of $\lesssim 1-2\times10^{-9}$ mbar. Samples were annealed from room temperature up to 1000°C. The released gases (e.g. H_2, HD, D_2, DT, T_2, and Be) were measured as a function of time and annealing temperature with a line-of-sight mounted, triple-filtered quadrupole mass spectrometer with pulse ion counting. The D signal was calibrated with similarly prepared D-implanted reference samples as was used for SIMS. The full results and the experimental setup for TDS are presented in Refs. [6, 21].

2. *Analyzed divertor tiles*

A full poloidal set of divertor tiles retrieved after ILW-1 have been analyzed, and the results have been reported extensively in previous publications (Refs. [3–8] and references therein). It was found, that with JET-ILW the D fuel retention process takes place via implantation and co-deposition, whereas in JET-C the D was found in massive C deposits, which covered large areas of the vessel wall. In ILW-1 the highest D retention values were found in regions with the highest deposition. These were located on top of the inner divertor on Tile 0 and on Tile 1 (Fig. 1). Lower retention was obtained in regions with thin impurity layers, or where implantation might be the main retention mechanism, i.e. in the base of divertor (Tiles 4 and 6), and on outer divertor (Tiles 7 and 8).

The analysis of divertor tiles retrieved after the ILW-2 campaign is ongoing [11–13, 21, 22]. This work discusses the results obtained from Tiles 1, 4, and 6, which have been exposed for single experimental campaign ILW-2. These tiles were prioritized in the analysis programme based on the results obtained from ILW-1 (highest deposition on Tile 1), and based on the plasma configuration and the resulted strike point locations on Tile 4 and 6 in ILW-2 (Fig. 2). Moreover, in addition to the divertor tiles being exposed only for ILW-2, tiles being exposed long-term for both ILW-1 and ILW-2 plasmas have been analyzed [11, 21, 22]. Here we report and compare results from the outer divertor (Tiles 6, 7 and 8) to results obtained from outer divertor tiles exposed only for ILW-1.

III. RESULTS

A. Inner divertor

In Fig. 3 are shown the measured poloidal distributions of the main impurities found on Tile 1 as obtained with 4.5 MeV NRA after ILW-1 and ILW-2. The result after ILW-1 campaign shows evidently the deposition and the D retention region being on the top horizontal part (apron), and on the upper vertical part of Tile 1 (Fig. 3(a)). This region is deep in the plasma

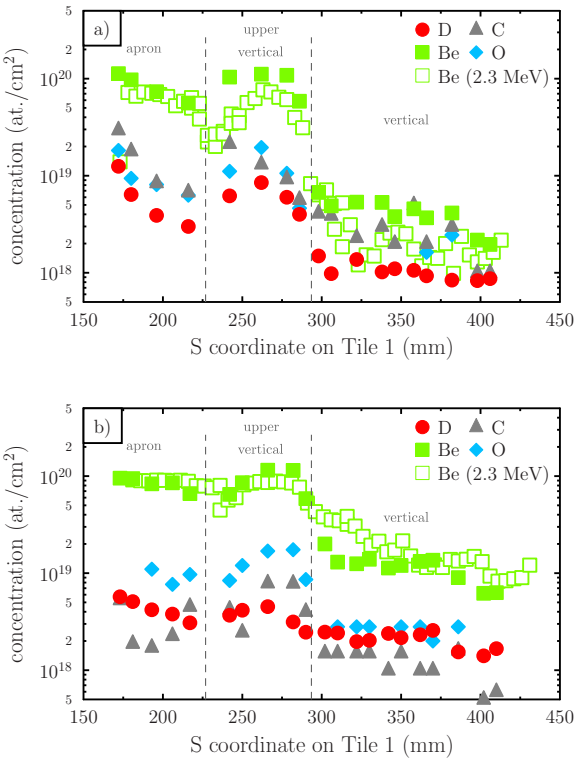

FIG. 3: (Color online) Poloidal distribution of the main impurities on Tile 1 as obtained with NRA using 4.5 MeV ^{3}He beam (also shown the Be result with 2.3 MeV ^{3}He). Fig. 3(a): NRA after ILW-1. High deposition on the apron (S = 162 . . . 227 mm) and on the upper vertical (S = 227 . . . 296 mm) surfaces. Significantly lower deposition and D fuel retention in the vertical region (S = 296 . . . 415 mm). Fig. 3(b): NRA after ILW-2. Top part of Tile 1 still with high deposition. A consiberable increase in deposition in the vertical part of tile. The D fuel retention is found to be almost homogenous along the tile.

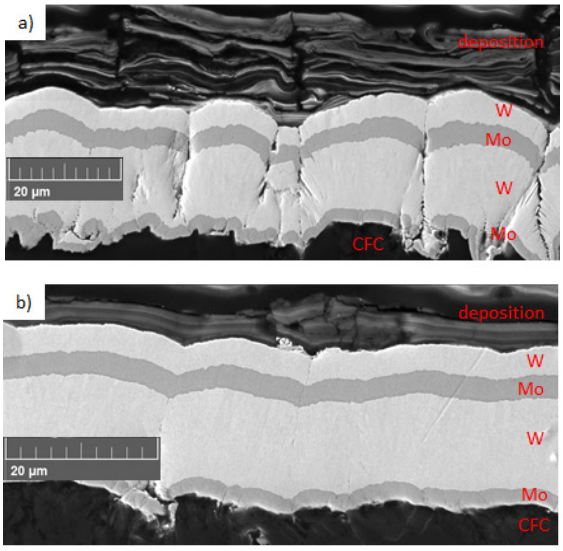

FIG. 4: SEM images on the deposition on Tile 1 apron (S = 216 mm) after one campaign exposures. Fig. 4(a): After ILW-1 a deposited layer of $10-15$ μm was formed. The deposition has a sandwich-like layered structure. Fig. 4(b): Formation of the deposited layer in ILW-2 has similar features as observed with the ILW-1 deposition.

scrape-off layer (SOL), and the D fuel is retained via co-deposition. The impurity layer is formed by the erosion of the main chamber Be limiters and the eroded particles being deposited on these horizontal surfaces. The thickness of $\sim 10^{20}$ Be/cm^2 corresponds to a deposit thickness of $10-15$ μm, as confirmed with tile profiling [3]. In ILW-1 the ISP was on Tile 3, and in ILW-2 it was predominantly on Tile 4. This resulted in shift of the SOL, which can be seen in the ILW-2 NRA results as a broader impurity distribution along Tile 1: the deposition is extended from the top horizontal part to the vertical region of Tile 1 (Fig. 3(b)) as the wider inner SOL allows particle transport into this area. The broadening of inner SOL nearly doubled the amount of Be and D in the vertical part of Tile 1 in ILW-2 ($\sim 10^{19}$ Be/cm^2, $\sim 2\times10^{18}$ D/cm^2) as compared to ILW-1 ($\sim 2-5\times10^{18}$ Be/cm^2, $\sim 10^{18}$ D/cm^2). However, the deposition thickness on the top horizontal part (apron) in ILW-2 remained the same as in ILW-1. This is seen also in the SEM images taken from the apron of Tile 1 (Fig. 4): the thickness and the layered sandwich-like structure formation appear to be similar in ILW-1 and in ILW-2. The origin on the formation of this structure plausibly correlates with the plasma interactions with the main chamber. Fig. 5 shows the SIMS impurity concentration profiles on the same region on Tile 1 apron as the SEM images. The ILW-1 SIMS profile for D shows a near-surface concentration peak (Fig. 5(a) subfigure). The ILW-2 was finished with a two-week H plasma campaign. The effect of the H operation can be seen as a decrease of the near-surface D concentration in the post-mortem SIMS analysis results. Fig. 5(b) shows the ILW-2 D concentration profile having near-surface dip extending up to ~ 0.5 μm in depth. The lack of D in this region correlates with the H being co-deposited in this region. Interestingly however, there is no visible D peak beyond 0.5 μm marking the end of the D operation. Thus it may concluded, that the D near-surface peak being potentially present in the end of D operations was replaced by a H peak in the start of the H operations, which was further affected by the continious H co-deposition in the course of the H campaign. The presence of retained near-surface H is seen in the poloidal D profile on Tile 1 after ILW-2: there are no evident D profile maxima along the tile, and on the top part of the tile (apron and upper vertical) the D retention has now similar values than what is found on the vertical region of the tile. Moreover, the effect of H seems to be crucial in the D retention in SOL deposits, since the amount of detected D after ILW-2 is approximately in the same order magnitude than what was detected after ILW-1 even though the amount of puffed D was two times higher in ILW-2 than in ILW-1.

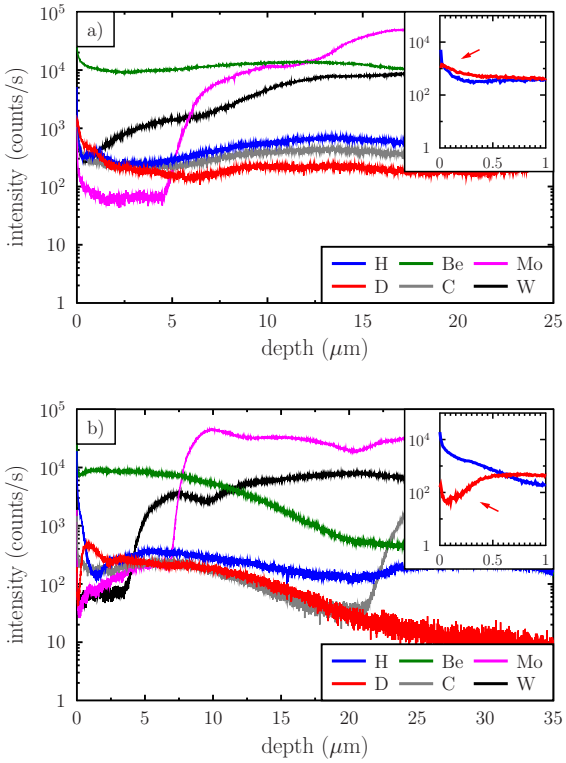

FIG. 5: (Color online) SIMS impurity concentration depth profiles for Tile 1 apron (S = 216 mm). Fig. 5(a): SIMS profiles after ILW-1. The subfigure shows a high near-surface D retention peak (highlighted by an arrow). Fig. 5(b): SIMS profiles after ILW-2. The near-surface D profile peak is missing (arrow) due to H co-deposition during the H plasma campaign in the end of ILW-2. The dip in the shape of the D profile extends up to ~ 0.5 μm from the sample surface.

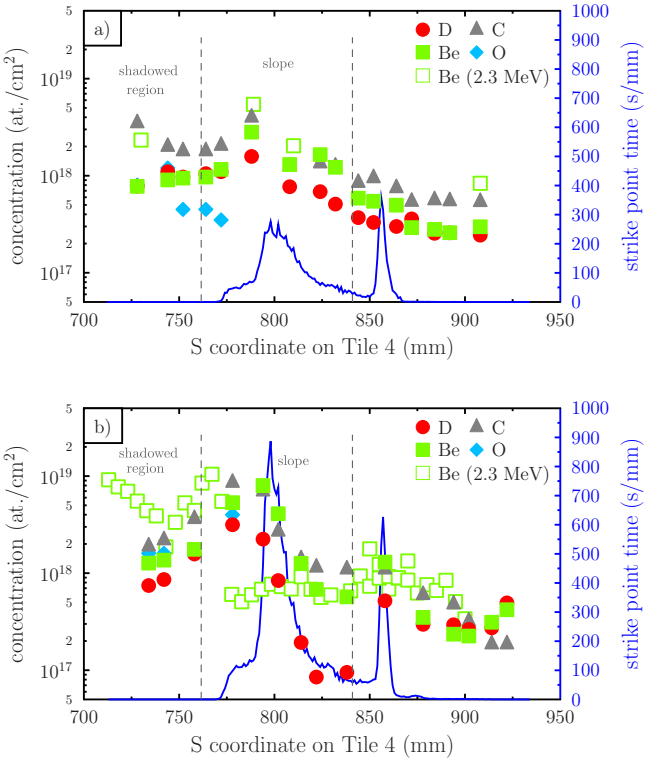

FIG. 6: (Color online) Poloidal distribution of the main impurities on Tile 4 as obtained with NRA using 4.5 MeV ^{3}He beam (also shown the Be result with 2.3 MeV ^{3}He). Also shown the strike point time along the tile. Fig. 6(a): NRA after ILW-1. Deposition is found on the sloping part (S = 762 . . . 840 mm) and in the shadowed region (S = 712 . . . 762 mm) of the tile. Deposition and D fuel retention increase outside the strike point area towards the shadowed region. Fig. 6(b): NRA after ILW-2. Increase in the deposition as compared to ILW-1 due to higher strike point time on Tile 4. The D fuel retention shows a decrease in the vicinity of the strike point induced heating. The D is found in the deposits outside the strike point.

Fig. 6 represents the NRA resolved impurity profiles along Tile 4 obtained after ILW-1 and ILW-2. In ILW-1 (Fig. 6(a)) the deposits are formed broadly around the strike point, and the D retention correlates with the deposition. In ILW-2 (Fig. 6(b)) the ISP was predominantly on Tile 4, which can be seen as an increase on the thickness of the deposit. The deposit is formed in the vicinity of the strike point and increasing towards the inner corner of the divertor. Due to higher input powers in ILW-2 (Table I) there is an obvious minimum in D retention at the ISP. This can be attributed to the elevated surface heat induced on Tile 4 due to higher powers and longer strike point time. In Ref. [23] it was shown the temperature rise reaching up to 1400°C at the strike points during a plasma discharge resulting in D outdiffusion from the tile surface and subsurface areas.

B. Outer divertor

The OSP was on Tile 5 in ILW-1 and on Tile 6 in ILW-2. Hence, after ILW-2 the deposition and the D retention patterns on Tile 6 have similar features as was observed on Tile 4 after ILW-2: the deposition is outside the strike point increasing towards the outer corner, and the D retention has a minimum value at the strike point. Fig. 7 shows SEM results obtained from the Tile 6 strike point location after ILW-1 and ILW-2. Since the strike point time on Tile 6 and the input power in ILW-1 were low, a thin deposited layer of few μm was able to be formed. In ILW-2, due to the high powers, the dominant strike point location and the resulted re-erosion events on Tile 6, the deposition at the OSP was found only in the microscopical plasma-shadowed regions, such as hills and valleys due to surface roughness. The subfigure in Fig. 7(b) shows the porous features observed on these remained deposit fractions. In Fig. 8 are shown the SIMS impurity depth profile results from the strike point region on Tile 6. In ILW-1 no thick deposit layers were formed (Fig. 8(a)), and the D retention was low ($\sim 10^{18}$

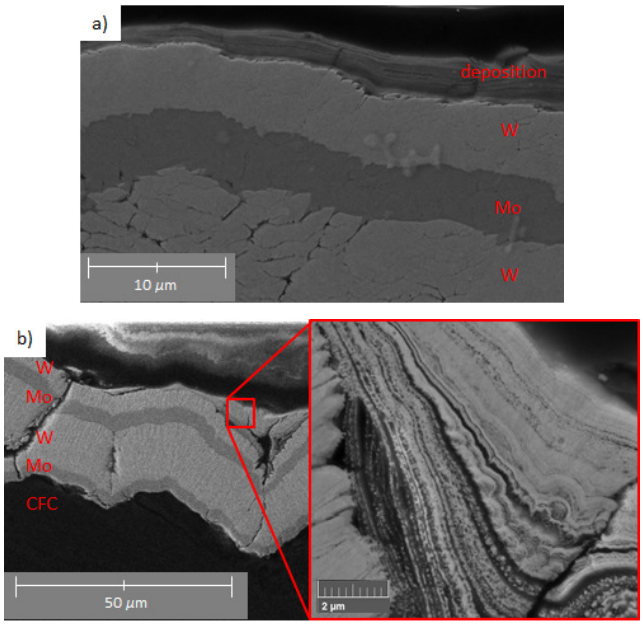

FIG. 7: SEM image on the deposition on Tile 6 sloping part (S = 1475 mm) after one campaign exposure. Fig. 7(a): After ILW-1 a layer of ∼few μm was formed. Fig. 7(b): During ILW-2 the location of the strike point at the sloping part resulted in re-erosion and in barely no deposition. Thin film formation is observed only in shadowed regions due to surface roughness. The magnification highlights the porous structure of these films.

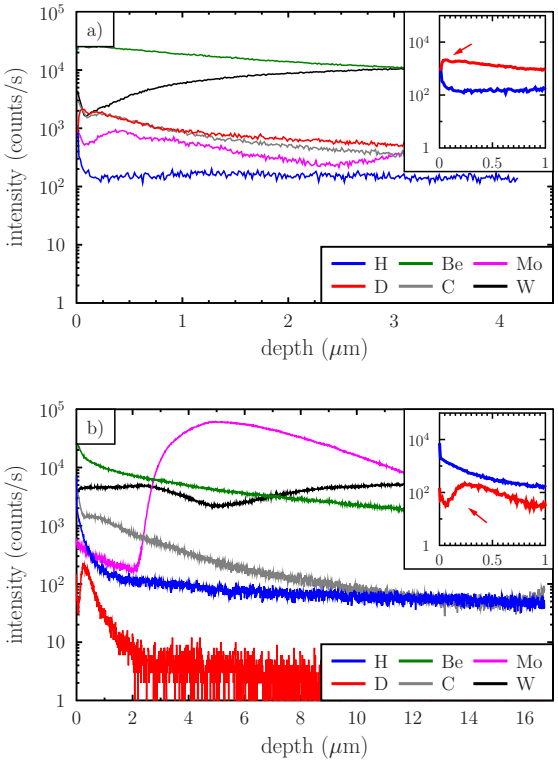

FIG. 8: (Color online) SIMS impurity concentration depth profiles for Tile 6 sloping part (S = 1475 mm). Fig. 6(a): SIMS profiles after ILW-1. The subfigure shows a clear near-surface D retention peak (arrow). Fig. 6(b): SIMS profiles after ILW-2. Similarly to Tile 1 apron (Fig. 4(b)) the near-surface D profile peak is missing (arrow). The H co-deposition during the H plasma campaign induced the dip to the shape of the D profile extending up to ~ 0.25 μm from the sample surface. The low D values in ILW-2 compared to ILW-1 are due to temperature effect of the high powers (Table I) and longer strike point time at the sloping part of Tile 6 in ILW-2 (Fig. 2).

D/cm^2). Due to the high heat on Tile 6 in ILW-2, the D amount was $1-2$ orders of magnitude less at the strike point (Fig. 8(b)). The ILW-1 SIMS profile for D shows a narrow near-surface profile peak (subfigure in Fig. 8(a)). The H campaign in the end of ILW-2 has an evident effect to the observed D depth profile. As was observed with Tile 1 (Sect. III A), the D on Tile 6 has a decreased near-surface concentration, which is seen as a dip in the D depth profile (up to ~ 0.25 μm in the bulk). However, the origin of this feature on Tile 6 may be different than on Tile 1. Due to the ILW-2 OSP being located on Tile 6 and because of lack of deposition at the strike point, the retained D can be considered originating mainly due to implantation. A similar feature in the change of the D near-surface profile has been also observed on ILW-2 Tile 5 samples, which were located in the private flux region and were without deposits [13].

Outer divertor tiles (Tiles 6, 7, and 8) being exposed to plasmas since the beginning of the ILW project (period 2011-2014; ILW-1 and ILW-2) were analysed with 4.5 MeV NRA, and the results were compared against corresponding outer divertor tiles exposed for ILW-1 only. Fig. 9 summarizes the main findings. During the ILW-1 there was no significant outer strike point induced heating affecting the D retention, and only minor amounts deposits were formed on Tiles 7 and 8 (Fig. 9(a)). The longer ILW exposure time 2011-2014, and the effect of the OSP being located on Tile 6 for longer time and with higher powers in ILW-2, had a significant effect on the D retention. As discussed, on Tile 6 a decrease in the D retention at the strike point region was observed, but a similar feature took place also on the bottom part of Tile 7 (Fig. 9(b)). Even though the Tile 7 strike point time was nearly identical in ILW-1 and ILW-2, the high power ILW-2 campaign resulted in increasing the D desorption during the ILW-2 plasma operations.

IV. SUMMARY AND CONCLUSIONS

To summarize, divertor fuel retention and deposition properties as obtained with ILW-2 post-mortem analyses have been compared with corresponding ILW-1 results. As in ILW-1, the top horizontal surface of the inner divertor remains in ILW-2 as the region with the thickest deposition formation. In ILW-1 the ISP was mainly on Tile 3.

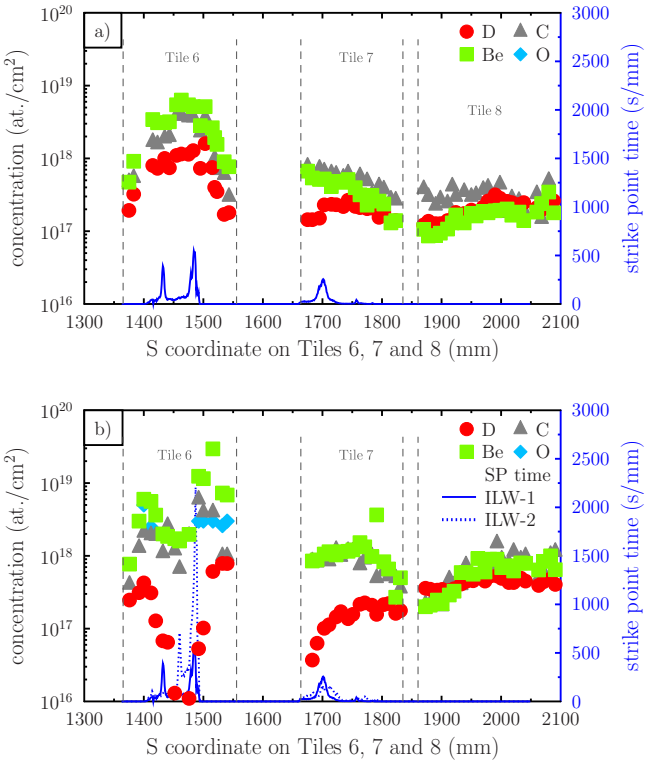

FIG. 9: (Color online) Poloidal distribution of the main impurities on Tiles 6, 7 and 8. Also shown the strike point time along the outer divertor. Fig. 9(a): NRA after ILW-1. Deposition and D fuel retention is found in the vicinity of the ILW-1 strike point on Tile 6. Fig. 9(b): NRA on tiles exposed for two campaigns ILW-1 and ILW-2. The deposition is increased on Tiles 7 and 8. On Tile 6 the two-campaign deposition shows an increase outside the strike point region. The D fuel retention shows a decrease at the strike points on Tiles 6 and 7 due to higher input power in ILW-2 (see Table I).

The ISP location in ILW-2 was on Tile 4, which widened the inboard SOL compared to ILW-1. This widening of SOL allowed thicker deposition formation further down on Tile 1. Moreover, due to higher input powers and increased erosion in ILW-2, more material migrated down to the divertor along the magnetic field lines. This was observed as an increase in the ILW-2 deposition on Tile 1 vertical surface and near the strike points on Tiles 4 and 6. However, the high power induced high heat at the strike point resulted in D outdiffusion during ILW-2 operation, which is seen as $1-2$ orders of magnitude lower D retention at the strike point as compared to ILW-1.

Unlike the ILW-1 campaign with D-only plasmas, the ILW-2 was finished with a two-week campaign of H pulses. Even though the total amount of puffed D was two times higher during ILW-2 than in ILW-1, the ILW-2 post-mortem results did not show correlation in D retention in the thick deposit region on top of the inner divertor. Instead, the h co-deposition resulted in near-surface accumulation of H instead of D, which was seen as a concentration dip in the measured D depth profile. This near-surface accumulation of H, and the resulting lack of near-surface D was observed poloidally throughout the divertor. However, the H implantation is expected to play a dominant role at the strike points, leading to a different mechanism for the change of hydrogen isotopes than in divertor areas with fuel co-deposition. In the co-deposited region on Tile 1, the D profile was affected by H up to 0.5 μm in depth, and at the strike point with implantation being the dominant retention mechanism up to 0.25 μm.

Analyses on outer divertor tiles being exposed for both ILW-1 and ILW-2 showed a nearly linear accumulation of deposition in regions outside of strike point. The D retention was observed to be strongly dependent on the ILW-2 strike point location. The high power operation enhances the D outdiffusion at the strike point, and fuel is found to be retained in the neighbourhood of the strike point. Deposit formation at the strike point in high power operation is decreased due to increased re-erosion processes.

The reported results are part of ongoing analysis work on ILW-2 and ILW-1 & ILW-2 exposed divertor tiles, and hence no global trends can be presently assessed. However, main differences originating from the ILW-1 and ILW-2 plasma operations are evident. Operating plasmas with higher powers lead to decrease in fuel retention and deposit formation at the strike points. Effect of H-only plasmas is seen as decrease of the D fuel retention in the near-surface regions of the plasma-facing components.

Acknowledgments

This work has been carried out within the framework of the EUROfusion Consortium and has received funding from the Euratom research and training programme 2014−2018 under grant agreement No 633053. The views and opinions expressed herein do not necessarily reflect those of the European Commission.

[1] G. F. Matthews, P. Edwards, T. Hirai, M. Kear, A. Lioure, P. Lomas, A. Loving, C. Lungu, H. Maier, P. Mertens, et al., Phys. Scripta **T128**, 137 (2007).
[2] S. Brezinsek, T. Loarer, V. Philipps, H. Esser, S. Grünhagen, R. Smith, R. Felton, J. Banks, P. Belo, A. Boboc, et al., Nucl. Fusion. **53**, 083023 (2013).
[3] A. Widdowson, E. Alves, C. F. Ayres, A. Baron-Wiechec, S. Brezinsek, N. Catarino, J. P. Coad, K. Heinola, J. Likonen, G. F. Matthews, et al., Phys. Scripta **T159**, 014010 (2014).

[4] J. P. Coad, E. Alves, N. P. Barradas, A. Baron-Wiechec, N. Catarino, K. Heinola, J. Likonen, M. Mayer, G. F. Matthews, P. Petersson, et al., Phys. Scripta **T159**, 014012 (2014).
[5] K. Heinola, A. Widdowsona, J. Likonen, E. Alves, A. Baron-Wiechec, N. Barradas, S. Brezinsek, N. Catarino, P. Coad, S. Koivuranta, et al., Phys. Scripta **T167**, 014075 (2016).
[6] J. Likonen, K. Heinola, A. D. Backer, S. Koivuranta, A. Hakola, C. F. Ayres, A. Baron-Wiechec, P. Coad, G. F. Matthews, and A. Widdowson, Phys. Scripta **T167**, 014074 (2016).
[7] M. Mayer, S. Krat, W. van Renterghem, A. Baron-Wiechec, S. Brezinsek, I. Bykov, P. Coad, Y. Gasparyan, K. Heinola, J. Likonen, et al., ps **T167** (2016).
[8] H. Bergsåker, I. Bykov, Y. Zhou, P. Petersson, G. Possnert, J. Likonen, S. Koivuranta, , and A. Widdowson, Phys. Scripta **T167** (2016).
[9] A. Widdowson, E. Alves, A. Baron-Wiechec, N. Barradas, N. Catarino, J. P. Coad, V. Corregidor, A. Garcia-Carrasco, K. Heinola, S. Koivuranta, et al., Nuclear Materials and Energy (2017), in press.
[10] A. Widdowson, A. Baron-Wiechec, P. Batistoni, E. Belonohy, J. P. Coad, P. Dinca, F. Fox, K. Heinola, I. Jepu, J. Likonen, et al., Phys. Scripta **T167**, 014057 (2016).
[11] A. Lahtinen, J. Likonen, S. Koivuranta, A. Hakola, K. Heinola, C. F. Ayres, A. Baron-Wiechec, J. P. Coad, A. Widdowson, and J. Raisanen, Nuclear Materials and Energy (2017), in press.
[12] N. Catarino, N. P. Barradas, V. Corregidor, A. Widdowson, A. Baron-Wiechec, J. P. Coad, K. Heinola, M. Rubel, and E. Alves, Nuclear Materials and Energy (2016), in press.
[13] S. Krat, M. Mayer, A. Baron-Wiechec, Y. Gasparya, K. Heinola, I. Jepu, C. Ruset, G. de Saint-Aubin, and A. Widdowson (2017), in preparation.
[14] E. Joffrin, M. Baruzzo, M. Beurskens, C. Bourdelle, S. Brezinsek, J. Bucalossi, P. Buratti, G. Calabro, C. Challis, M. Clever, et al., Nucl. Fusion. **54**, 013011 (2014).
[15] F. Romanelli and on behalf of JET Contributors, Nucl. Fusion. **55**, 104001 (2015).
[16] M. Mayer, *SIMNRA User's Guide 6.05* (Max-Planck-Institut für Plasmaphysik, Garching, Germany, 2009), http://home.rzg.mpg.de/ mam/index.html.
[17] S. Krat, M. Mayer, I. Bykov, C. P. Lungu, G. de Saint Aubin, A. Widdowson, and I. S. Carvalho, Nuclear Materials and Energy **11**, 20 (2017).
[18] N. P. Barradas and C. Jeynes, Nucl. Instr. Meth. Phys. Res. B **266**, 1875 (2008).
[19] J. Likonen, E. Alves, A. Baron-Wiechec, S. Brezinsek, J. P. Coad, A. Hakola, K. Heinola, S. Koivuranta, G. F. Matthews, P. Petersson, et al., Phys. Scripta **T159**, 014016 (2014).
[20] K. Heinola, T. Ahlgren, E. Vainonen-Ahlgren, J. Likonen, and J. Keinonen, Phys. Scripta **T128**, 91 (2007).
[21] J. Likonen, K. Heinola, A. D. Backer, S. Koivuranta, C. F. Ayres, A. Baron-Wiechec, P. Coad, I. Jepu, G. F. Matthews, and A. Widdowson (2017), in preparation.
[22] M. Mayer, S. Krat, A. Baron-Wiechec, Y. Gasparyan, K. Heinola, S. Koivuranta, J. Likonen, C. Ruset, G. de Saint-Aubin, and A. Widdowson (2017), in preparation.
[23] S. Brezinsek, S. Wiesen, D. Harting, C. Guillemaut, A. J. Webster, K. Heinola, A. G. Meigs, M. Rack, Y. Gao, G. Sergienko, et al., Phys. Scripta **T167**, 014076 (2016).